Department of
Mechanical Engineering

Colorado State University

An Investigation of Electrohydrodynamic Heat Pipes

R. I. Loehrke

Mechanical Engineering Department

Colorado State University

Fort Collins, Colorado 80521

March 1977

Final Report

NASA Grant #NGR-06-002-127

Prepared for

Ames Research Center

National Aeronautics and Space Administration

Moffett Field, California 94035

The work described in this report was performed under NASA Grant NGR-06-002-127, "An Investigation of Electrohydrodynamic (EHD) Heat Pipes." This program was conducted at Colorado State University with Dr. T. B. Jones and Dr. R. I. Loehrke as principal investigators. The NASA Technical Officer for this grant is Dr. C. McCreight, NASA Ames Research Center, Moffett Field, California, 94035.

CR-151,977

An Investigation of Electrohydrodynamic Heat Pipes

R. I. Loehrke

Mechanical Engineering Department

Colorado State University

Fort Collins, Colorado 80521

March 1977

Final Report

NASA Grant #NGR-06-002-127

Prepared for

Ames Research Center

National Aeronautics and Space Administration

Moffett Field, California 94035

Contents

PART I - CURRENT STATUS

1. The EHD Heat Pipe Concept

The electrohydrodynamic (EHD) heat pipe, as proposed by Jones,[1] utilizes the force exerted on a dielectric fluid in a non-uniform electric field to form liquid channels[2,3] connecting the condenser and evaporator sections of a heat pipe. These channels function as low resistance arteries through which liquid may flow from the condenser to the evaporator during heat pipe operation. A sketch of one possible channel configuration (the one employed in all of the experiments to be described) is shown in Figure 1. In this configuration the axial rods (electrodes) are maintained at a high voltage with respect to the grounded heat pipe shell. The liquid phase of the dielectric working fluid collects in the high field strength region forming a tent-like open channel between the condenser and evaporator ends of the pipe. In response to heat transfer the liquid-vapor interface at the evaporator end of the heat pipe recedes into the high field strength region while the interface at the condenser end bulges out into the lower field strength area giving rise to a net pumping head which drives the liquid from the condenser to the evaporator. The role of the electric forces in the EHD heat pipe is analogous to that of surface tension forces in a capillary heat pipe. In steady state operation the electrical current required to maintain the tent flow structure is negligible.

The basic principles governing EHD heat pipe operation have been detailed by Jones.[4,5] The polarization or dielectrophoretic force acting on a dielectric fluid in a non-uniform electric field can be viewed as a surface traction acting at the interface between the liquid and vapor. This surface traction supports a pressure differential across the interface,

the net effect being somewhat analogous to that produced by surface tension in a capillary tube. The maximum pressure difference, due to electrical forces, available to drive liquid from the condenser to the evaporator is,

$$\Delta p_e = \frac{\varepsilon_\ell - \varepsilon_o}{2} E^2_{max} .$$

Under static conditions these forces can lift the liquid against gravity to a height given by

$$h_s = \frac{(\varepsilon_\ell - \varepsilon_o) E^2_{max}}{2\rho_\ell g} \qquad (1)$$

During heat pipe operation the height to which the liquid can be raised is reduced due to flow related pressure losses in the fluid circuit. The maximum electric field strength which can be sustained is limited by the breakdown strength of the working fluid. For the electrode structure shown in Figure 1, $E \sim V/S_{AS}$. Since the size of the liquid return channel, for a given E, scales with S_{AS} it is limited only by the available voltage level and by geometric constraints. Thus the viscous flow losses in the liquid channel can be minimized without reducing the available pumping head.

Although the EHD heat pipe can be operated without any sort of capillary wicking, and indeed surface tension forces were ignored in the above discussion, in most of the experiments a capillary structure was employed to distribute the liquid over the evaporator surface. In the proof of concept experiment performed by Jones and Perry[6] the axial electrode structure was mated with an internally threaded pipe. This heat pipe was operated with both A.C. and D.C. electric fields demonstrating the dielectrophoretic[2] nature of the phenomenon. Heat pipe operation was also achieved in a tube in which an axial electrode was coupled with a Feltmetal

capillary liner.[7] Other experiments, to be reviewed later, indicate that, depending on the application, capillary assist may not be required.

2. Applications

In light of the fact that the two essential requirements for operation of an EHD heat pipe are the use of a dielectric working fluid and the availability of a high voltage source it appears that a natural application of this device would be for cooling of electrical equipment. In this application it may be desirable to combine the element to be cooled and the heat pipe structure into an integral unit. Even in situations in which a high voltage source is not available it may be worth investing in one to take advantage of the special features offered by the EHD heat pipe. These features are outlined in the following paragraphs.

Because of the inherent uncoupling between maximum pumping head and arterial size mentioned earlier the EHD heat pipe affords relatively high thermal throughput. Where the operating temperature range or other considerations dictate the use of a dielectric working fluid the EHD approach may represent the low technology solution to a design problem. In order to match its thermal capacity using a conventional heat pipe complex capillary structures may be required. The comparison drawn by Loehrke and Debs[8] illustrates this point although recent experiments by Saaski[9] indicate that high-performance wicks need not be arterial.

In contrast to capillary driven arteries, EHD arteries offer positive priming under load. Experiments have documented that priming can be achieved even in presence of nucleate boiling.[6, 10] Vapor bubbles are ejected from the open tent-like arteries as the liquid advances over the hot evaporator surface. Capillary priming follows arterial priming as the surface in the vicinity of the tent is cooled.

Since the location of the liquid inventory is determined primarily by the combination of gravitational and electric forces voltage controlled conductance can be realized.[10] With the evaporator end of the heat pipe elevated above the condenser end in a gravitational field the conductance can be varied from a maximum (evaporator surface fully wetted) to near zero (evaporator surface dry) by simply varying the voltage level supplied to the axial electrodes. Under the inverse orientation additional electrodes covering only the condenser end of the heat pipe would be energized to hold the liquid against the gravitational pull.

Another feature of the EHD heat pipe is that no wick or special surface geometry is required. Although capillary wicking has generally been assumed to be a necessary element in an EHD heat pipe, the experiments described in Part II of this report reveal that the average evaporator unit conductance is degraded only slightly when a grooved active surface is replaced by a smooth one. Thus, in applications where the heat rejecting surface is inviolate the EHD approach is still valid. No special surface preparation or blanketing wick is required.

3. Performance

Two important performance measures, maximum throughput and conductance, have been studied. Although these measures are not strictly independent, the coupling between them, for the range of EHD configurations investigated, has proven to be remarkably weak. The basic mechanisms which establish the limits to thermal throughput appear, at this time, to be better understood than those which govern the conductance. The following paragraphs summarize the results of several performance studies of EHD heat pipes of the general configuration shown in Figure 1.

Maximum Thermal Throughput

Given a basic EHD structure, e.g., three, symmetrically placed axial rod electrodes within a pipe of a given diameter, there are remaining two geometric variables, rod diameter and rod-wall spacing, and voltage which may be selected to optimize the heat pipe performance. If the optimization involves maximizing throughput based purely on hydrodynamic considerations then that maximum flow rate will be determined by one of the following limits:[4]

1. Sonic limit - as in conventional pipes.
2. EHD surface wave celerity limit - which places a constraint on the maximum liquid flow velocity.
3. Entrainment limit.
4. Pumping limit - analogous to the wicking limit in capillary pipes.

Which of these limits sets the maximum flow rate depends on the working fluid, operating temperature range, geometry and voltage. Constraints on these variables enter as:

1. Voltage supply limits.
2. Vapor breakdown voltage limit.
3. Fluid freezing point and critical point or decomposition limits.

The last constraint couples the maximum throughput to the conductance, however, the coupling noted in capillary pipes due to the onset of nucleation is not experienced in EHD pipes.

The pumping limit referred to above pertains to the capacity of the axial EHD arteries. In designs where capillary structures form a significant part of the evaporator surface liquid distribution system (see the next section) then the capacity of this system may limit the throughput.

A working fluid figure of merit proposed by Jones[4]

$$N_{EHD} = \frac{(\varepsilon_\ell - \varepsilon_o)\, h_{fg}\, E_b^2}{\nu_\ell} \qquad (2)$$

based on the pumping limit (as set by the liquid viscous pressure loss) and the vapor breakdown constraint may be helpful in selecting candidate working fluids.

Liquid entrainment by the counterflowing vapor is a potentially more severe problem in an EHD pipe with its open arterial configuration than in a conventional arterial pipe. Jones and Perry[11] analyzed this problem and experimentally verified their analysis. They present criteria for the onset of entrainment and suggestions for postponing onset should such measures be necessary.

The EHD wave speed limit[4] is unique to EHD heat pipes. In the open channel arterial flows a condition of criticality is reached when the velocity of the liquid approaches the surface wave celerity. This condition is interpreted as limiting the liquid flow rate through the artery. Experimental and theoretical determinations of wave speed for the tent geometry are described by Jones and Melcher.[3]

In all of the EHD heat pipes built and tested to date the maximum throughput has been pumping limited. None of these pipes were optimized for maximum throughput in the sense described by Jones,[4] but rather the geometry and working fluid were chosen for experimental convenience. On the other hand, by virtue of the fact that most of these pipes were operated near the vapor breakdown limit, the heat transfer rates are representative of the maximum attainable for that geometry, working fluid and voltage supply limit.

Of particular interest are the results reported by Loehrke and Debs[8] obtained with a 30 cm long circular EHD pipe. At the time that paper was written it was not clear that dryout had been attained in any of the experiments. Subsequently Debs[12] tested a 114 cm long version of this pipe which clearly demonstrated dryout behavior.

The long pipe is identical to the short pipe described in reference 8 except for two changes. First, the adiabatic section was lengthened and second, four Teflon spacers, 0.25 cm thick, were used for internal support of the three axial rod electrodes. These spider-like spacers, Figure 2, were relieved in the areas between the rods and the wall to minimize flow resistance. The facilities and techniques used in testing this pipe were identical to those described in reference 8. The working fluid was again R-11.

One experiment was run, at a tilt angle of 0.56 degrees, to the point where the evaporator dryout signature was unmistakable. A plot of average evaporator superheat versus power level for this run is shown in Figure 3. The onset of dryout, as characterized by the sudden change in slope, was accompanied by fluctuations in some of the evaporator surface temperatures similar to those noted by Loehrke and Debs[8] with the short pipe at the highest tilt and highest power. Taking this to imply that incipient dryout had been reached in that earlier experiment the dryout data in Table I were compiled.

Table I

Conditions at Dryout

	30 cm pipe @ 3°49' tilt.		113 cm pipe
L' (cm)	15.24		96.52
h (cm)	2.29	3.10	1.64
q_{max} (w)	95-100	0	28-38
$q_{max}L'$ (w-cm)	1448-1524	0	2703-3668
V (kv)	16	16	16

The values for h presented here are calculated vertical distances from the top of the excess liquid puddle at the condenser end of the pipe to the topmost point at the evaporator end of the pipe. The value for h at $q_{max} = 0$ was calculated based on the observed electrode voltage required to depress the temperatures at the uppermost evaporator thermocouple during startup (See reference 8). The observed h was then extrapolated to 16 kv using equation 1. The effective length of the heat pipe L' is measured from the center of the evaporator to the center of the condenser.

A plot of the dryout data is shown in Figure 4. The nearly straight line correlation is characteristic of pumping power limited throughput. Order of magnitude calculations reveal that the liquid supply viscous losses are dominant. Precise analytical corroboration is difficult because:

a) the precise tent geometry is unknown.

b) the liquid frictional characteristics of the open tent with counterflowing vapor at the surface is unknown.

c) the three electrodes are not at the same elevation and thus are pumping against different gravitational heads.

The last difficulty could be accommodated but the first two preclude ar accurate analysis.

With the flexibility available to the designer of an EHD heat pipe (voltage level, number, size and shape of electrodes, etc.) the numbers presented here could be easily altered and in fact considerably higher throughput estimates are given by Jones[4] for optimized pipes. On the other hand, it is unlikely that the hydrodynamically optimized pipe will be the best choice for most applications. Conductance related limits may take precedence. At any rate, the circular pipe data establishes an experimental benchmark against which other designs can be compared.

Conductance

EHD heat pipe conductance (or its constituent parts, evaporator conductance or overall heat transfer coefficient, $U_e = \frac{q}{A_e \Delta T_e}$, and condenser conductance, $U_c = \frac{q}{A_c \Delta T_c}$) has been the subject of a number of investigations.[6,7,8,10] This summary will be limited to those determinations of conductance which were not obviously biased by condenser flooding due to excess inventory or by partial evaporator dryout due to pumping limitations of either the EHD arterial structure or capillary distribution system. With that qualification one can draw the following tentative conclusions based on the limited amount of data available:

1) EHD heat pipe conductance is comparable to that obtained in conventional heat pipes with grooved active surfaces using the same working fluid.[8]
2) Condenser conductance is about double evaporator conductance.[8]

3) Evaporator conductances in EHD heat pipes having no capillary structures are nearly as high as those measured in grooved surface pipes. (See Part II of this report.)

In terms of numbers, measured EHD evaporator conductances have ranged from 0.07 to 0.16 w/cm^2-°C using R-11 as working fluid.[8,10]

Because of the unknown nature of the basic heat transfer mechanisms in the liquid layer covering the EHD heat pipe evaporator surface, it is likely that these conclusions will remain tentative for some time to come. The conventional conduction model for transport through the liquid layer does not adequately explain the observations. There is evidence that this model may also be deficient in certain capillary heat pipes of unconventional geometry.[9] The possibility that surface tension variations due to temperature variations over the liquid-vapor interface may drive convection was investigated. As reported in Part III of this report there is insufficient information available to make a judgment on this possibility.

The conclusions drawn earlier and the conductance values quoted are all for relatively low evaporator superheat. Experiments[8,10] with R-11 working fluid have shown that at high enough superheats ($\Delta T_e \approx 10°C$ for these tests), nucleate boiling begins in the vicinity of the EHD tents and the average evaporator conductance increases appreciably. Thus, in contrast to conventional capillary heat pipes where nucleate boiling adversely affects heat pipe operation, EHD heat pipes may be profitably operated in the ebullient regime.

4. Open Questions

The two major unanswered questions concerning the performance of EHD heat pipes involve long term materials compatibility or fluid degradation in presence of strong electric fields and the previously raised issue of conductance.

Since the EHD heat pipe is constrained to operate using fluids having notoriously poor thermal conductivies and since the experimental results to date indicate that conductance rather than throughput may limit performance it would be desirable to have a better understanding of the processes which control the conductance. Fundamental studies aimed at uncovering these processes would benefit the development of heat pipes in general, particularly those operating in temperature ranges requiring use of similar low conductivity fluids.

PART II - EVAPORATOR CONDUCTANCE EXPERIMENTS

1. Introduction

Previously reported EHD heat pipe experiments have indicated that the adverse effects of the thick, liquid tents on evaporator conductance may not be as severe as expected. An analysis, based on a conduction model for heat flow through the liquid layer, of the evaporator of the heat pipe tested by Loehrke and Debs revealed that the evaporator surface superheat beneath the EHD tents should have been about 30% higher than that at between-tent locations prior to the onset of groove dryout.[13] That the observed circumferential surface temperature distributions were not consistent with this analysis would tend to indicate that the conduction model is not appropriate. Similarly, the experiments of Loehrke and Sebits[10] showed little degradation of evaporator conductance due to arterial shielding. Loehrke and Debs hypothesized that under certain circumstances, namely for isothermal evaporator surfaces, capillary grooves may not be required in EHD heat pipes.

The aim of the experiments reported here was to test this hypothesis. A heat pipe was designed and constructed in which grooved and ungrooved evaporator surfaces can be interchanged to provide a direct comparison of evaporator conductances. In addition, the electrode density in this pipe can be varied over a wide range. This flexibility provided the opportunity to obtain design data concerning the optimum electrode spacing.

2. Experiments

The EHD heat pipe used in these experiments is similar to the one described in reference 8. In this flat plate geometry the evaporator and condenser surfaces lie in a plane. The vapor space above this plane is

covered with a transparent plate to facilitate observation of the EHD tents. A view of this heat pipe, looking down through the transparent cover, is shown in Figure 5. Identical active surfaces, each 10.16 cm wide and 12.07 cm long (in the flow direction), are separated by a 5.5 cm adiabatic section. Suspended 0.32 cm above these grounded surfaces are 15, 0.16 cm diameter, rod electrodes spaced on 0.64 cm centers. Any number of these electrodes can be energized to a high D.C. potential for a given test. This provides the flexibility to vary the fraction of the active surfaces which is covered by EHD tents. Additional flexibility has been provided by making the active surfaces removeable. Two sets of evaporator and condenser surfaces were used in these experiments. One set, shown installed in Figure 5, was grooved while the other was smooth.

The heat pipe enclosure consists of three major parts, shown in Figure 6, which are bolted together. The cover is a 1.27 cm thick polished Lexan plate. The center section, a hollowed out 2.54 cm thick Lexan plate, forms the vapor chamber. The base plate, also of Lexan, holds the active surfaces and adiabatic section and completes the enclosure. A Lexan frame, which fits completely within the enclosure, is used to support the electrodes. The base plate has been machined so that the upper surfaces of the evaporator, condenser and adiabatic section lie in the same plane.

The evaporator is formed from a brass plate to the back of which is glued a heating unit. Two different evaporator plates were made, one smooth and 0.32 cm thick and one grooved and 0.23 cm thick. Both have eight #2-56 studs brazed to the bottom surface near the outer edge. The grooves are approximately square in cross-section, 0.08 mm deep and cut to a density of 3.85 mm^{-1}. The groove profiles are shown in Figure 3 of reference 10. The heating unit was formed by sandwiching a 0.64 cm thick

plexiglas plate with thermocouples imbedded on both sides between two sheets of Armstrong Temsheet resistance heating material. The heating element closest to the evaporator surface forms the main heater while the other one serves as a guard heater. The heating unit, measuring 10.48 cm by 8.57 cm was then epoxied to the bottom of an evaporator plate.

The plates which form the condenser surfaces are identical to the evaporator plates. Heat is removed from the condenser section of the heat pipe by passing coolant from a constant temperature circulating bath through tubes attached directly to the lower surface of the brass condenser plates. Five 36-gage copper-constantan thermocouples are attached to each active surface at the locations shown in Figure 7.

The active surfaces were sealed to the base plate with Dow-Corning 733 RTV flourosilicone rubber. The adiabatic section was covered with a layer of 0.013 mm thick aluminum foil which was bonded to the Lexan with the same adhesive. The studs attached to the brass plates extend through the Lexan base plate. Nuts were placed on these studs and tightened, after the rubber had cured, to provide additional support for the active surfaces.

The Lexan harp which forms the electrode support structure serves not only to hold the rods in position but also carries the load required to maintain tension in the 15 electrodes. The threaded ends of the rods pass through holes in the harp. Nuts are turned onto the rods and tightened down until the desired tension is achieved. This fastening arrangement limited the spacing between electrodes to a minimum of 0.64 cm. At closer spacings arcing between adjacent rods occurred when alternate electrodes were grounded. Based on this electrode spacing the gap between the electrodes and the base plate was set at 0.32 cm. so that when all electrodes

are energized the EHD tents will cover virtually the entire active surface. Shorting straps were designed to fit under the fastening nuts and connect together all electrodes which are to be energized and all which are to be grounded so that only two electrical feed-throughs are required for the heat pipe enclosure. Two additional holes were drilled through the center section. One, to which a valve was attached, served as a fill port. A thermocouple probe was inserted through the other to measure vapor temperature.

Two series of experiments were performed, one with smooth active surfaces and one with grooved active surfaces. In each experiment the temperatures of the active surfaces, the vapor temperature and the power to the main heater were recorded. In all experiments the working fluid was R-11. The aim of these experiments was to obtain quantitative information concerning the influence of electrode spacing and active surface geometry on the conductance of an EHD heat pipe. All of the data presented, however, are concerned just with evaporator conductance for the reasons outlined in the next paragraph.

Because of the relatively large spacings between the electrodes and the active surfaces used in these experiments, compared to the diameter of the electrode rods, a significant concentration of electric field strength occurred in the vicinity of the electrodes. Thus, the field strength at the surface of the evaporator, which determines the useful EHD pumping head, was about a factor of three lower than the maximum field strength near the electrodes. For this reason the maximum tilt which could be achieved without breakdown was relatively small. Under most operating conditions at these low values of tilt the condenser surface was flooded with a pool of excess liquid which reduced the condenser conductance to about one third the level of the evaporator conductance. Since this condition is not typical in

well-designed heat pipes, see for example reference 8, it was felt that these condenser conductance values were not meaningful. It should be emphasized that this test pipe was designed for maximum experimental flexibility and was not optimized for overall conductance.

3. Results

For all of the experiments reported here the electrode voltage was maintained at 12.5 kv D.C. and the heat pipe tilt, evaporator over condenser, was set at one degree. The data are presented in terms of average evaporator superheat, ΔT_e, as a function of net heat throughput or main heater power, q, and as evaporator conductance, U_e at equilibrium conditions.

A plot of evaporator superheat versus power for several different electrode configurations with smooth active surfaces is shown in Figure 8. These data show a relatively small change in evaporator conductance for a large change in amount of evaporator surface covered by tents. Visual observation indicated that one possible reason for the small effect noted was that the tent shape, and thus the amount of surface covered by the tent, depended on the liquid inventory. With a large inventory the actual vertical lift which had to be overcome by the EHD forces was small so the tents were broad and covered a large portion of the evaporator surface. With a reduced inventory the tents would be forced to recede into the high field strength region directly below the electrodes to provide the extra lift and thus the amount of evaporator surface covered was smaller. The same effect is observed with a constant inventory if the tilt is changed.

In order to better pinpoint the effect of tent geometry on evaporator conductance subsequent experiments were performed to find the maximum

conductance for a given electrode configuration. This was done by fixing the heater power and varying the inventory. Each test was initiated with an extra large inventory, the heater power was fixed at 25 watts and the average evaporator conductance at equilibrium was measured. A small amount of R-11 was then removed from the pipe by opening the fill valve for a short period of time. Conductance was again measured after equilibrium was re-established. The results of one such test are shown in Figure 9. Equilibrium point one corresponds to the condition of maximum inventory. At this inventory, with the electrodes not energized, a pool of liquid covered the entire condenser and adiabatic section. At the last equilibrium point, number nine, a substantial portion of the evaporator surface was dried out. For the test configuration represented in Figure 9 the maximum conductance occurred at about the point where the EHD tents were thinnest, but still fully primed. The maximum single point conductance, determined in this way, for a range of electrode densities is shown in Table 1. for both smooth and grooved evaporator surfaces.

Table 1.

Maximum Evaporator Conductance

Surface Finish	Electrode Density (cm^{-1})	U_e (w/cm^2-°C)	Percent Surface Covered by Tent
Smooth	1.575	.075	56
	.787	.086	68
	.524	.067	50
Grooved	1.575	.097	43
	.787	.100	23
	.524	.103	--
	.394	.085	--

The absolute maximum conductance for both grooved and ungrooved surfaces occurred at an electrode density less that 1.575 cm^{-1} (every electrode energized) which would seem to indicate some insulating effect of the liquid tent. However, especially for the grooved surfaces, the variation of maximum conductance with electrode density is extremely small. Surprisingly, the highest conductance measured with the ungrooved surface is only about 15 percent lower than that for the grooved surface.

An attempt was made to quantify the effect of inventory change on the liquid tent structures by determining the fraction of the evaporator surface that was covered by liquid at each equilibrium point. Photographs of the evaporator surface were taken at each point and the area covered by the tents was measured from these pictures using a planimeter. For the smooth plates this gives a measure of the total area covered by liquid, however, for the grooved plates it measures only the area covered by the tents. The extent to which the grooves were wetted could not be assessed visually under equilibrium conditions. The photograph reproduced in Figure 10 shows the smooth evaporator surface under maximum conductance conditions with every electrode energized. The adiabatic section is to the right and the bright regions to the left represent dried out sections of the evaporator surface. Variations in the tent widths due to small differences in the spacing between the electrodes and plate can be seen. In fact, the third electrode from the top is partially unprimed at this operating point. Plots of evaporator conductance versus fraction of evaporator surface covered by liquid tents, such as those presented in Figure 11, revealed that the maximum conductance with the smooth evaporator surface were attained with over half the evaporator surface covered with

liquid. With the grooved evaporator surface the maximum conductance was achieved with less than one half of the surface covered by liquid tents. For the grooved surface with every electrode energized many of the tents were partially unprimed at the point of maximum conductance. Clearly, the grooves were supplying liquid to a larger fraction of the evaporator surface than was covered by the tents. This also accounts for the fact that the maximum conductance listed in Table I for this configuration was comparable to that measured for the condition of every other electrode energized.

To summarize, the visual observations of the EHD tent structures coupled with thermal measurements showed that the evaporator conductance, for both the grooved and ungrooved surfaces, was about 0.04 to 0.05 w/cm^2-°C when the entire surface was covered by the liquid tents. As the liquid inventory was reduced and the tents receded under the electrodes the conductance increased for both surfaces. The maximum conductance for the smooth evaporator surface was achieved when the area covered by the tents was reduced to about 50 - 80% of the total evaporator surface area. The highest conductance, 0.086 w/cm^2-°C, was attained with every other electrode energized. At this point the energized electrodes were fully primed with liquid. In contrast, with the grooved evaporator surface the conductance continued to increase with decreasing inventory until a maximum value was reached with about 20 to 40% of the evaporator area covered by liquid tents. The maximum conductance of 0.103 w/cm^2-°C was observed with every third electrode energized and fully primed.

These observations indicate that the grooves were effective in distributing liquid over the evaporator surface between arterial tents. This was confirmed by visual observation. Although the liquid could not be

detected in the grooves under equilibrium conditions under transient conditions, for example when the high voltage to the electrodes was suddenly turned off, groove dryouts could be observed.

The fact that the conductance for the grooved surface changed by only a factor of three when the fraction of evaporator area covered by the liquid tents changed from 100% to 20% lends support to the hypothesis that convection processes are augmenting heat transfer through the tents. This contention is reinforced by the relatively high conductance measured for the smooth surface. A two-dimensional numerical conduction model of the smooth evaporator surface and EHD tent structure was analyzed and the results showed one possible alternative explanation for the high conductance values noted. If heat were transferred strictly by conduction through the liquid layer then in order to realize the observed average conductance level virtually all of the heat loss from the evaporator must occur in the thin edge layer near the junction between the tent and the dried out region of the evaporator surface. The exact geometry of the tent in this region is difficult to acertain. One would expect, however, a strong correlation between the measured conductance values and the length of this junction or interline present on the evaporator surface if this did represent the principal region of heat transfer. The length of this interline was measured from the photographs taken of the smooth evaporator surface at the various levels of inventory. These lengths and the corresponding measured conductances are plotted in Figure 12. The absence of any clear correlation suggests that this mechanism alone cannot be responsible for the total heat transfer to the liquid.

4. Conclusions

These experiments have shown that an EHD heat pipe can operate effectively without the need for capillary structures, such as grooves, to aid in distributing liquid over the evaporator surface. Comparison tests showed that smooth evaporator surfaces gave average conductances only 15% lower than surfaces with capillary grooves. The conductance of the grooved surface was, however, less sensitive to variations in the spacing between electrodes.

For the smooth evaporator surface the maximum conductance of 0.086 w/cm^2-°C was attained when the spacing between adjacent electrodes was four times the spacing between the electrode and the active surface. For the grooved surface the optimum spacing ratio was between four and six and the maximum measured conductance was 0.103 w/cm^2-°C.

Strong evidence was obtained to suggest that the heat transfer through the liquid layer covering the evaporator surface is augmented by convection.

PART III - CONVECTION IN THIN FILMS

1. Introduction

Analytical estimates of heat pipe conductance have traditionally been based on conduction models for heat transfer through the liquid layers in the evaporator and condenser. The rationale for neglecting cross-film mixing motions has been that the characteristic dimensions of the liquid films confined by capillary structures are small so that the stabilizing actions of viscosity and heat conduction overpower any driving forces arising from temperature gradients in the film. In many applications this assumption may be perfectly valid. If it is not, however, conductance estimates may be overly conservative and analytically derived geometric optimizations may not be pertinent. In particular, it appears that this assumption may not be valid for certain EHD heat pipe designs.

There are at least three possible driving mechanisms for heat convection in evaporating liquid layers (in absence of nucleation within the liquid). The terms buoyancy-driven convection, surface-tension-driven convection and electroconvection may be used to classify the motion according to the dominant driving force. The first depends on the presence of an acceleration field, the last on an electric field while the second is ubiquitous. In an EHD heat pipe all three mechanisms may be important. Criteria for determining whether or not convection will occur and, if it will, what will be the effect on heat transfer depend strongly on geometry and boundary conditions. A great majority of the experimental and analytical work which has been published relevant to thin film convection deals with horizontal fluid layers of uniform depth. Although the results of this work are not directly applicable to most heat pipe geometries they can provide a guide to the

relative importance of the various mechanisms and shed some light on potential problem areas. It is significant that even for this well-studied geometry a completely verified coupled theory accounting for just buoyancy plus surface tension effects does not exist. The following sections focus on convection in horizontal layers. A number of review papers have been published which offer a broader perspective on this problem.[14,15,16,17]

2. Convection in Horizontal Fluid layers.

Of the three mechanisms for driving convection mentioned previously the one associated with buoyancy forces has been subject to more analyses which have been verified by experiment than either of the other two. These have shown that when a horizontal layer of fluid is heated from below in a gravity field convection begins, due to the destablizing density gradient, at a critical value of the Rayleigh number, $Ra = \frac{g\beta\Delta TL^3}{\nu\alpha}$, which depends on the thermal and hydrodynamic boundary conditions. Experiments with conducting upper and lower rigid boundaries are in good agreement with the theoretical prediction for critical Rayleigh number. Theoretical predictions for the critical Rayleigh number have been made for a variety of idealized boundary conditions including all combinations of free and rigid upper and lower boundaries and perfectly conducting and perfectly insulated (to temperature perturbations) upper and lower boundaries. The critical values range between $320 \leq Ra \leq 1708$. Sufficient experimental results have been reported which are not in disagreement with these predictions that the linear theory on which they are based is well accepted. The heat flux through the layer, for fixed ΔT, has been found to undergo a transition from being inversely proportional to layer depth for subcritical conditions to being virtually independent of layer depth for supercritical conditions.

One of the reasons that this mechanism is well documented is that it is relatively easy to design an experiment in which the critical parameter, Ra, can be accurately measured and in which alternate mechanisms are eliminated. This clean separation is not possible in surface-tension and electroconvection experiments.

In a horizontal layer consisting of two superposed fluids separated by an interface convection may be induced by surface (interface) motions driven by surface tension variations due to temperature or concentration perturbations. In spite of the fact that this is basically a two-layer, two-fluid problem most analyses are patterned after Rayleigh's single-fluid model for buoyancy driven convection. This model gives rise to a parameter, the Marangoni number $Ma = \frac{\sigma' \Delta T L}{\rho \nu \alpha}$, which, in absence of gravity, describes the convection boundary. As with the critical Rayleigh number, the critical Maragoni number depends on the boundary conditions of the fluid layer but, in contrast, the possible range is much larger. For example, for a conducting, rigid lower boundary and a free upper boundary the critical Marangoni number ranges from $80 \leq Ma \leq \infty$ as the upper thermal boundary ranges from perfectly insulating to perfectly conducting. Although sufficient experimental evidence exists to confirm that surface tension forces can drive convection the quantitative agreement between theory and experiment found for buoyancy driven convection is lacking. This subject is reviewed in more detail in the next section.

Convection, in the EHD heat pipe, may also be driven by body forces attributable to the strong electric field. One of these forces, the dielectrophoretic force, is responsible for the formation of the liquid arterial structure in the EHD heat pipe. Even in a single phase fluid this

force may be present and due to property (permittivity) variations with temperature. The effect is somewhat analogous to that due to density variations in a gravitational field. Savkar[18] found that, in absence of gravity, convection will begin in a dielectric fluid layer, confined between parallel conducting plates maintained at a potential difference ΔV and temperature difference ΔT, at a critical value of "dielectrophoretic Rayleigh number" $ER = \frac{\varepsilon C}{\nu K} (\gamma \Delta T \Delta V)^2 \simeq 2.4 \times 10^3$. Turnbull[19] has analyzed the combined dielectropheric and gravity problem in a horizontal layer heated from below and predicted a marked destabilizing effect due to electric field. Turnbull and Melcher[20] have demonstrated that the destabilizing effect of dielectrophoretic forces can be strong enough to overcome a stabilizing density gradient. They observed and predicted convection under conditions of negative gravitational Rayleigh number. It is interesting to note that Savkar's critical ER is independent of layer depth. Using the property values for R-11 we can estimate a critical value for the product of voltage difference times temperature difference above which convection should take place in a horizontal layer as $\Delta T \Delta V \simeq 30 \times 10^3$ [v-°C]. Although not directly applicable to the heat pipe geometry the magnitude lies within the range in which all of the EHD pipes have been operated. In D.C. fields Coulomb forces on free charges may also be important and, in fact, are usually the dominant cause of electroconvection. The relative magnitude of the dielectrophoretic force compared with the Coulomb force is given by $\frac{\phi}{\varepsilon} \frac{d\varepsilon/dT}{d\phi/dT}$.[21]

For the general horizontal layer with a free surface in an electric field convection may be driven by the coupled action of the forces due to gravity, surface tension and electric field. Uncoupled analyses indicate

that the relative importance of these forces will depend on layer depth. For a given fluid and with fixed electric field strength the critical ΔT for onset of convection due to buoyancy forces varies as $1/L^3$ while for surface tension and electroconvection in absence of gravity ΔT_c varies as $1/L$. Thus, buoyancy forces should be relatively less important for thin layers. Whether or not surface-tension or electric field forces ever become large enough to drive convection will depend on the details of the problem. The importance of surface-tension forces in evaporative convection appears to be particularly difficult to assess at this time. A brief review of this problem is presented in the next section.

3. Surface-Tension Driven Convection in Horizontal Layers.

There is sufficient theoretical and experimental evidence to support the contention that surface tension variations can induce convection in fluid layers.[14] Quantitative comparisons between theoretical predictions and experimental results are, however, sparse in contrast to the state of affairs for buoyancy driven convection. Virtually no experimental data are available for evaporating layers of a pure liquid. A review of the theoretical and experimental attempts to determine the conditions required for the onset of convection in a horizontal layer will serve to indicate where the difficulties lie with respect to drawing conclusions concerning evaporating layers.

The most thoroughly studied configuration consists of two horizontal immiscible fluid layers separated by an interface characterized by a surface tension the magnitude of which depends on temperature. The earliest studies focussed on fluids having vastly different densities and viscosities and treated the problem in terms of a single fluid with a free boundary. The

governing equations were linearized for small perturbations to the initial quiescent condition with constant temperature gradient. The thermal conditions at the free boundary were characterized in terms of a Biot number $\frac{HL}{k}$. $Bi \to \infty$ corresponds to an iosthermal boundary while $Bi = 0$ represents a boundary with a fixed mean heat flux, i.e. insulated to perturbations in heat flux. Pearson[22] found that in absence of gravity convection will begin at a critical value of the Marangoni number Ma, the magnitude of which depends on the Biot number. Nield[23] extended Pearsons analysis to include the effects of gravity. His results indicated a strong coupling between the buoyancy and surface tension effects with a suppression of the critical ΔT required for the onset of convection when the layer is heated from below and complete stabilization when the layer is heated from above. The difficulty in applying the results of these analyses enters in the determination of the Biot number at the free surface for a practical configuration.

Smith[24] circumvented the requirement for setting a thermal boundary condition at the interface by analyzing the two-fluid problem. He obtained a closed-form solution for the critical Marangoni number, in absence of gravity, which depends only on the properties of the two fluids and on the surface tension variation with temperature. Zeren and Reynolds[25] extended the two-fluid analysis to include the effects of gravity. Both of these analyses indicate that convection may occur not only with heat addition from below but also, for certain fluid combinations, with heating from above.

One of the main uncertainties associated with all of the linear analyses mentioned above is that the principle of exchange of stabilities has been assumed without proof. That is, convective motions are assumed to result only

from perturbations which grow monatonically in time. Sternling and Scriven[26] have shown, however, that for deep layers, in absence of gravity, oscillatory modes may be unstable. If oscillatory modes are possible in finite layers then convection may begin at Marangoni numbers lower than those predicted by extant linear theories. So far, no such modes have been observed experimentally.

Although Grodzka[27] has reported observations of cellular convection in essentially zero gravity conditions all of the quantitative data available which can be used to check the theories has been obtained in presence of a gravitational field. Thus, one must relate these results to theories in which the effects of buoyancy are included. Zeren and Reynolds[25] performed experiments with benzene-water layers and qualitatively verified certain aspects of their theory. They were, however, unable to produce the predicted convection with heating from above or to obtain the predicted magnitude of coupling when the layers were heated from below. They attributed these discrepancies to uncertainties in the surface tension which is extremely sensitive to minute levels of contamination.

While the analysis of Zeren and Reynolds appears to be the most general performed to date for combined buoyancy and surface-tension effects the price paid for this generality is that a simple, closed form solution for the stability boundary cannot be obtained. Each configuration must be analyzed individually and the stability criteria determined by numerical methods. On the other hand, the more restricted analysis of Nield yields a simple criterion for the stability boundary but requires knowledge of the interfacial thermal boundary condition. Koschmieder[28] performed experiments with layers of silicone oil and air and reported qualitative agreement with Nield's theory. He inferred values for the interfacial boundary conditions from measurements of the wavelengths of the roll cells formed just after the

onset of convection. Palmer and Berg[29] and Hoard[30] et al. performed similar experiments and found good agreement with Nield's theory using an interfacial boundary Biot number estimated on the basis of a one-dimensional conduction model. Based on these limited experimental data it appears that Nield's theory can be used to predict the onset of convection for certain fluid combinations and geometries specifically those in which the shear stresses in upper fluid layer are negligible and also deformations of the interface are negligible.

4. Evaporating Liquid Layers.

Heat transfer coefficients at evaporating interfaces are generally quite high and, in fact, interfacial thermal resistance is typically neglected in estimating heat pipe conductance. If the interfacial heat transfer coefficient is high then the potential for sustaining surface temperature variations and thus surface tension variations is low. If one assumes that, at least for low evaporation rates, Nield's predictions apply to layers with net vapor production then the liquid layer temperature drop required for the onset of surface-tension driven convection should be quite high. At low pressures or with non-condensible gases present in the vapor phase, however, Sukhatme and Rohsenow[31] have shown that the interfacial resistance can be appreciable. Indeed, the only reported observations of surface-tension driven convection in evaporating layers of pure liquids have been for net evaporation into a non-condensible gas.[32] Under normal heat pipe operating conditions, however, it does not seem likely that the interfacial resistance would be high enough to support convection.

In layers with non-planar interfaces it is possible that surface temperature variations may be produced due to the influence of surface curvature on the equilibrium vapor pressure.[33] Thus, in heat pipes with capillary evaporator structures it is conceivable that convection within the capillary pore could be present if the interface radius of curvature were not constant. On the other hand the presence of the confining side-walls should tend to inhibit convection.[34] At the present time there is insufficient information available to assess the importance of surface-tension driven convection in general heat pipe applications. However, in the EHD heat pipe experiments with a smooth evaporator surface reported in Part II surface-tension driven convection was probably not important. Interfacial radii of curvature were large and non-condensible gases, if present, were swept away from the evaporating interface reducing the possibility for surface temperature variations.

Reference

1. Jones, T. B., "Dynamics of Electromechanical Flow Structures," Ph.D. Thesis, Dept. of Electrical Engineering, M.I.T., August 1970.

2. Castle, J. N., "Dielectrophoresis," Tech. Report LG-5, Dept. of Mech. Engr., Stanford Univ., December, 1967.

3. Jones, T. B. and Melcher, J. R., "Dynamics of Electromechanical Flow Structures," Phys. Fluids, Vol. 16, No. 3, p. 393, 1973.

4. Jones, T. B., "The Feasibility of Electrohydrodynamic Heat Pipes," Res. Report No. 1, NASA CR-114392, Elec. Engr. Dept., Colorado State University, October, 1971.

5. Jones, T. B., "An Electrohydrodynamic Heat Pipe," Mech. Engr., Vol. 96, No. 1, 1974.

6. Jones, T. B. and Perry, M. P., "Experiments with an Electrohydrodynamic Heat Pipe," Res. Report No. 3, NASA CR-114498, Elec. Engr. Dept., Colorado State University, September, 1972.

7. Jones, T. B. and Perry, M. P., "Electrohydrodynamic Head Pipe Research," Res. Report No. 4, NASA CR-114646, Elec. Engr. Dept., Colorado State University, July, 1973.

8. Loehrke, R. I. and Debs, R. J., "Measurements of the Performance of an Electrohydrodynamic Head Pipe," AIAA paper 75-659, 10th Thermophysics Conference, May, 1975.

9. Saaski, E. W., "Investigation of an Inverted Meniscus Heat Pipe Wick Concept," NASA CR-137,724, August, 1975.

10. Loehrke, R. I. and Sebits, D. R., "Flat Plate Electrohydrodynamic Heat Pipe Experiments," NASA CR-137707, Mech. Engr. Dept., Colorado State University, July, 1975.

11. Jones, T. B. and Perry, M. P., "Entrainment in Electrohydrodynamic Heat Pipes," Res. Report No. 2, NASA CR-114499, Elec. Engr. Dept., Colorado State University, August, 1972.

12. Debs, R. J., Private communication.

13. Day, W. J., "Influence of Geometry on an Evaporating Surface in an Electric Field," M.S. Thesis, Mech. Engr. Dept., Colorado State University, 1977.

14. Berg, J. C., Acrivos, A. and Boudart, M., "Evaporation Convection," Advances in Chemical Engineering, Vol. 6, p 64, 1966.

15. Scriven, L. E. and Sternling, C. V., "The Marangoni Effects," Nature, Vol. 187, p. 186, 1960.

16. Whitehead, J. A., "Cellular Convection," American Scientist, Vol. 59, p. 444, 1971.

17. Koschmieder, E. L., "Benard Convection," Adv. in Chem. Physics, Vol. 26, p. 177, 1974.

18. Savkar, S. D., "Dielectrophoretic Effects in Laminar Forced Convection Between Two Parallel Plates," Physics of Fluids, Vol. 14, p. 2670, 1971.

19. Turnbull, R. J., "Effect of Dielectrophoretic Forces on the Benard Instability," Physics of Fluids, Vol. 12, p. 1809, 1969.

20. Turnbull, R. J. and Melcher, J. R., "Electrohydrodynamic Rayleigh-Taylor Bulk Instability," Physics of Fluids, Vol. 12, p. 1160, 1969.

21. Turnbull, R. J., "Electroconvective Instability with a Stabilizing Temperature Gradient II. Experimental Results," Physics of Fluids, Vol. 11, p. 2597, 1968.

22. Pearson, J.R.A., "On Convection Cells Induced by Surface Tension," J. Fluid Mech., Vol. 4, p. 489, 1958.

23. Nield, D. A., "Surface Tension and Buoyancy Effects in Cellular Convection," J. Fluid Mech., Vol. 9, p. 341, 1964.

24. Smith, K. A., "On Convective Instability Induced by Surface-Tension Gradients," J. Fluid Mech., Vol. 24, p. 401, 1966.

25. Zeren, R. W. and Reynolds, W. C., "Thermal Instabilities in Two-Fluid Horizontal Layers," J. Fluid Mech., Vol. 53, p. 305, 1972.

26. Sternling, C. V. and Scriven, L. E., "Interfacial Turbulence: Hydrodynamic Instability and the Marangoni Effect," AIChE Journal, Vol. 5, p. 514, 1959.

27. Grodzka, P. G. and Bannister, T. C., "Heat Flow and Convection Demonstration Experiments Aboard Apollo 14," Science, Vol. 176, p. 506, 1972.

28. Koschmieder, E. L., "On Convection Under an Air Surface," J. Fluid Mech., Vol. 30, p. 9, 1967.

29. Palmer, H. J. and Berg, J. C., "Convective Instability in Liquid Pools Heated From Below," J. Fluid Mech., Vol. 47, p. 779, 1971.

30. Hoard, C. Q., Robertson, C. R. and Acrivos, A., "Experiments on the Cellular Structure in Benard Convection," Int. J. Heat Mass Trans., Vol. 13, p. 849, 1970.

31. Sukhatme, S. P. and Rohsenow, W. M., "Heat Transfer During Condensation of a Liquid Metal Vapor," J. Heat Transfer, p. 19, 1966.

32. Berg, J. C., Boudart, M. and Acrivos, A., "Natural Convection in Pools of Evaporating Liquids," J. Fluid Mech., Vol. 24, p. 721, 1966.

33. Potash, M. and Wayner, P. C., "Evaporation from a Two-Dimensional Extended Meniscus," Int. J. Heat Mass Transfer, Vol. 15, p. 1851, 1972.

34. Bentwich, M., "Buoyancy and Surface-Tension Induced Instabilities of Fluid in Open and Closed Vertical Cylindrical Containers," Appl. Sci. Res., Vol. 14, p. 305, 1971.

Nomenclature

A = surface area

$Bi = HL/k$ - interfacial Biot number

C = specific heat

E = electric field strength

$ER = \frac{\varepsilon C}{\nu k} (\gamma \Delta T\ \Delta V)^2$ - dielectrophoretic Rayleigh number.

g = acceleration of gravity

h = vertical height of liquid rise

h_{fg} = heat of vaporization

H = interfacial heat transfer coefficient

k = thermal conductivity

L = layer depth

L' = effective length of heat pipe

$Ma = \frac{\sigma' \Delta T L}{\rho \nu \alpha}$ - Marangoni number.

N_{EHD} = working fluid figure of merit (Eqn. 2)

p = pressure

q = heat flow rate

$Ra = \frac{g \beta \Delta T L^3}{\nu \alpha}$ - Rayleigh number.

S_{AS} = spacing between electrode and heat pipe surface

S_E = spacing between energized electrodes

$U = q/A\Delta T$ - conductance

V = voltage

α = thermal diffusivity

β = thermal expansion coefficient

γ = thermal coefficient of permittivity

ΔT = temperature difference

ε = electrical permittivity

ν = kinematic viscosity

ρ = density

σ = surface tension

σ' = change in σ with temperature

ϕ = electrical conductivity

Subscripts

ℓ = liquid

v = vapor

e = evaporator

c = condenser

b = breakdown

o = free space.

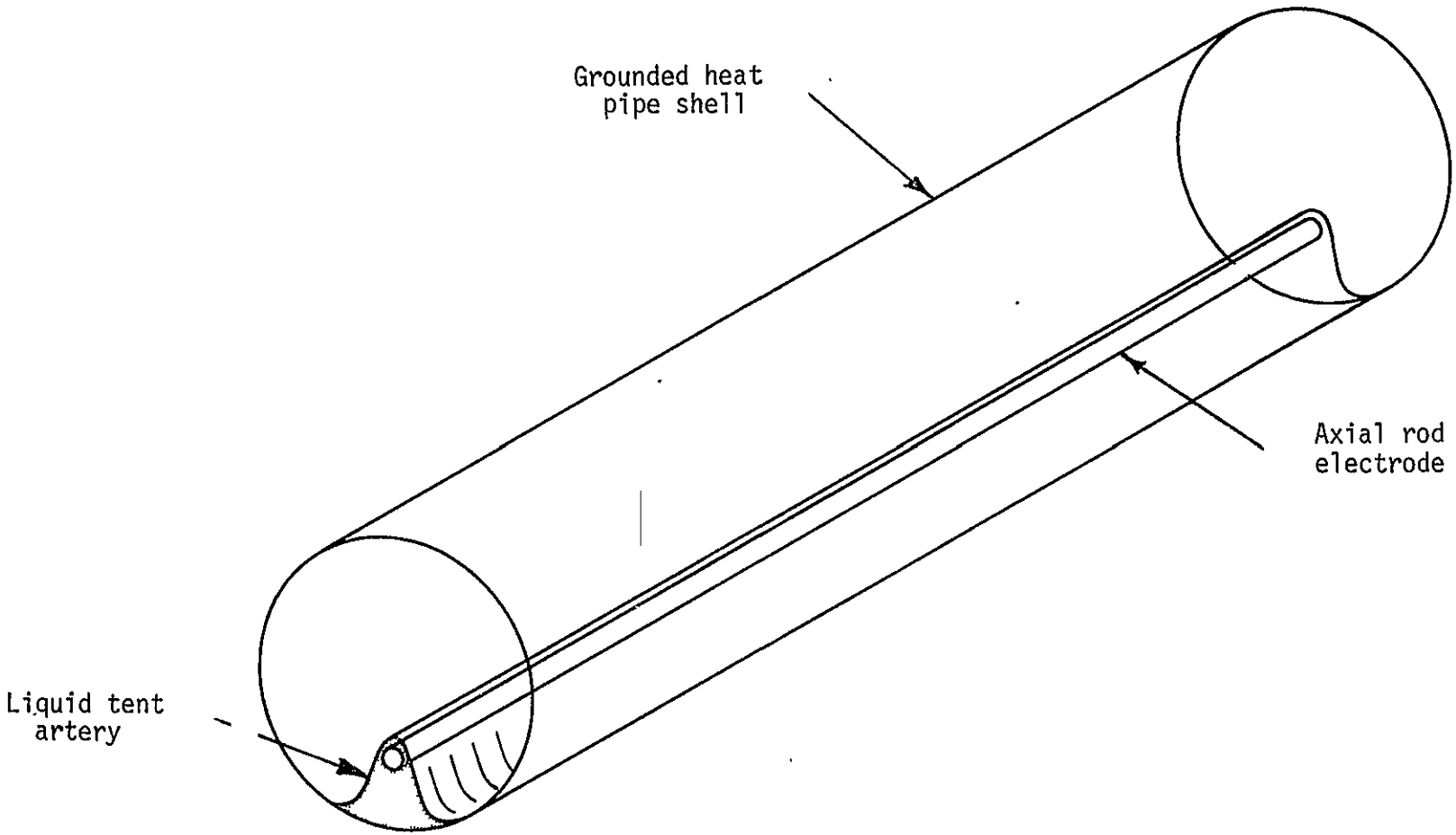

Figure 1. EHD Heat Pipe Schematic

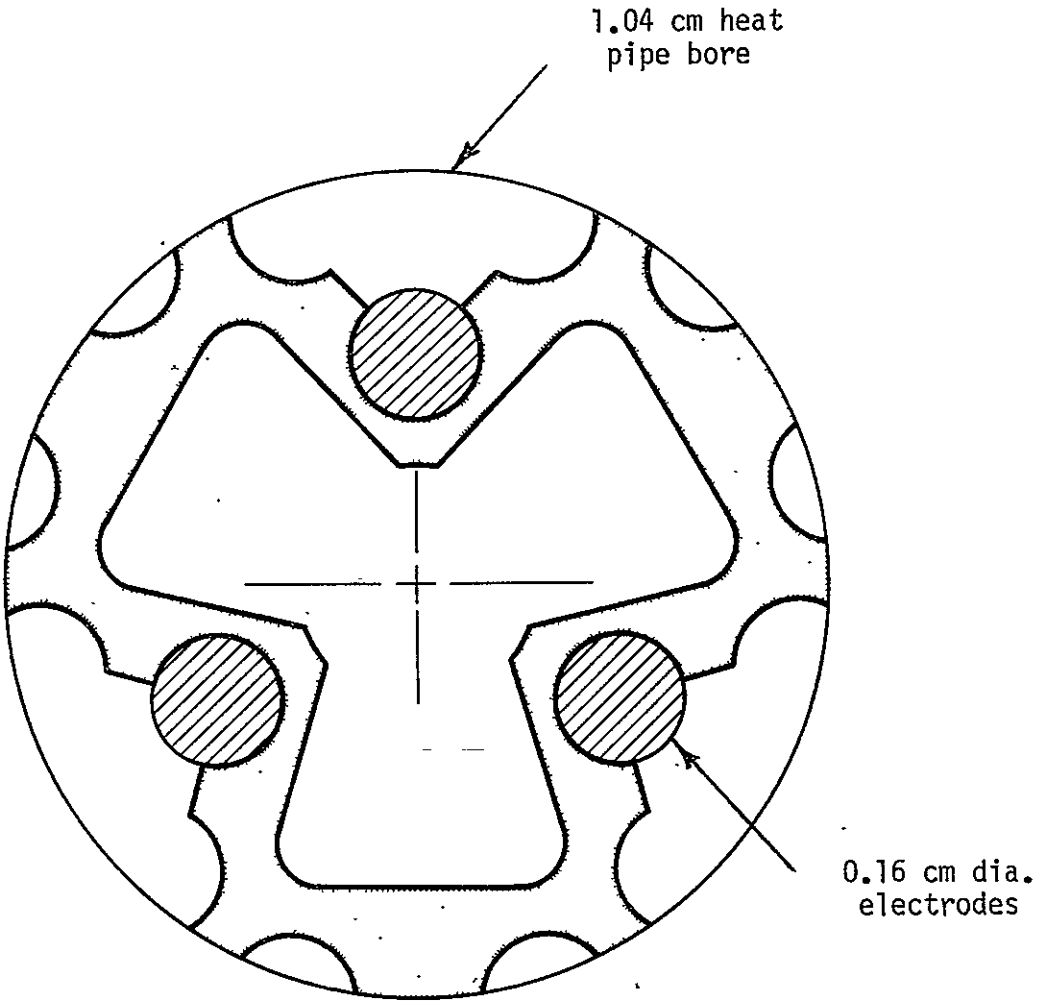

Figure 2. Sketch of 0.25 cm thick Teflon spacer (shaded) used to support electrodes

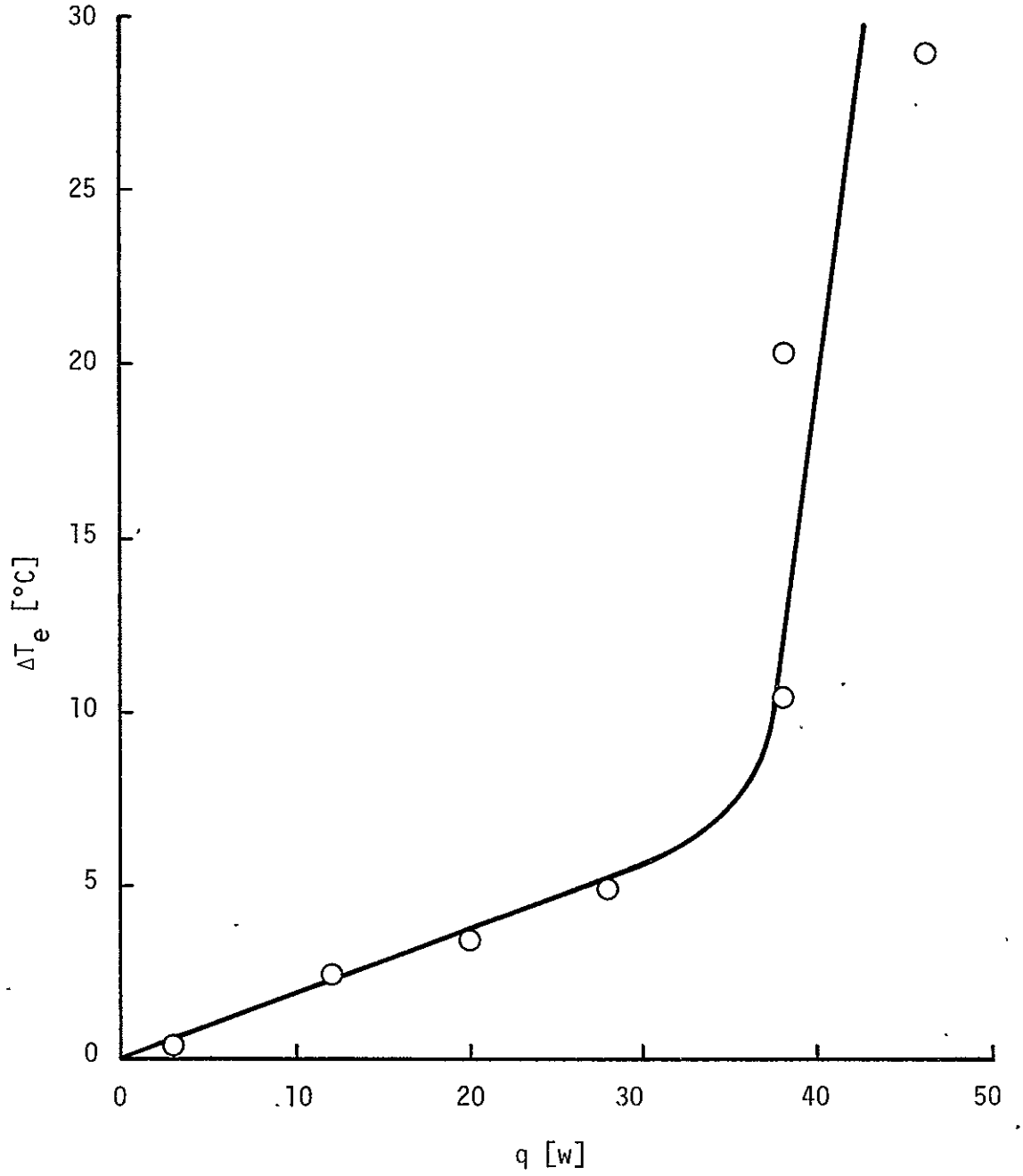

Figure 3. Evaporator Superheat versus Power for the 114 cm Long Heat Pipe.[12]

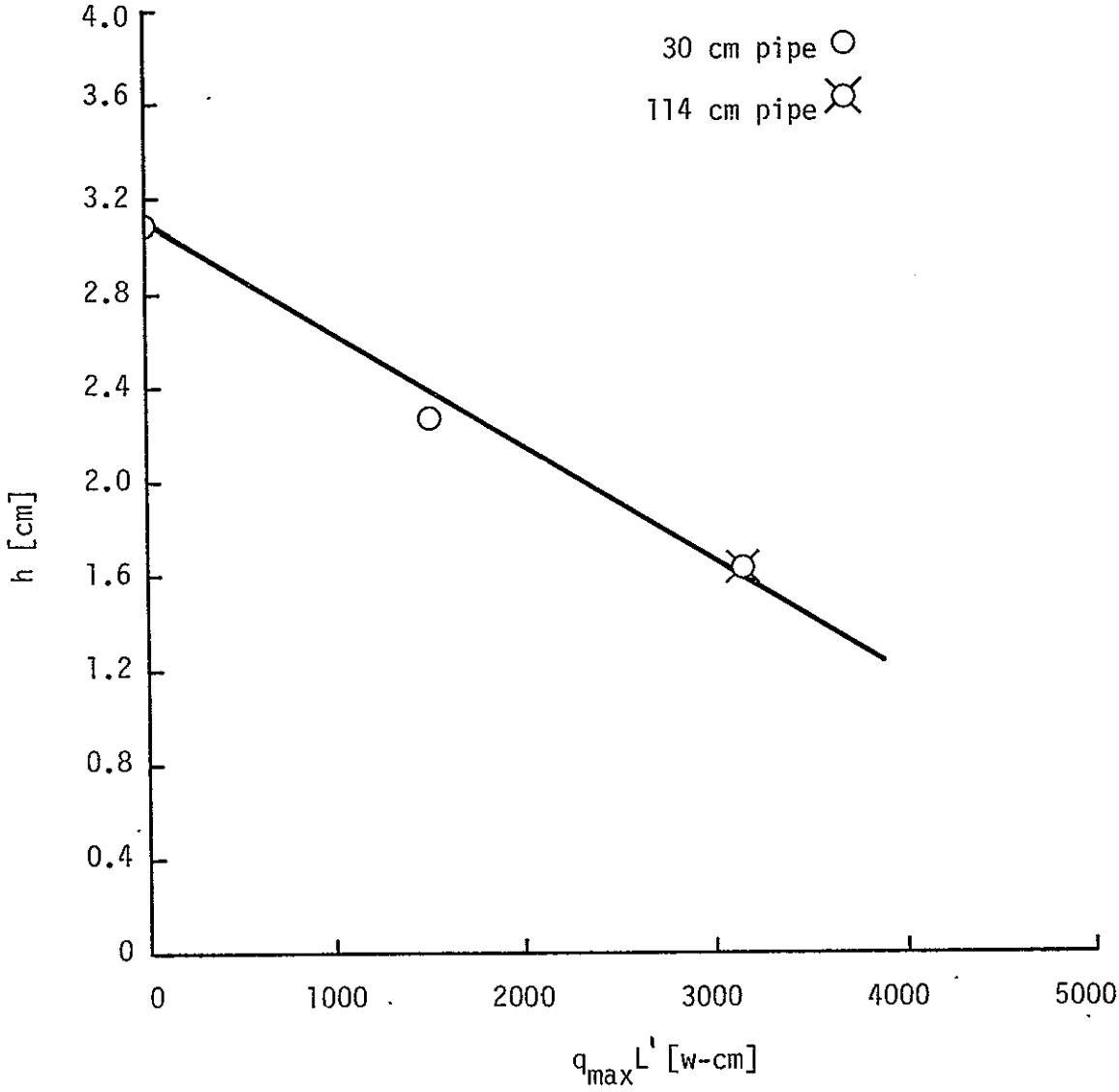

Figure 4. Conditions at the Onset of Dryout.

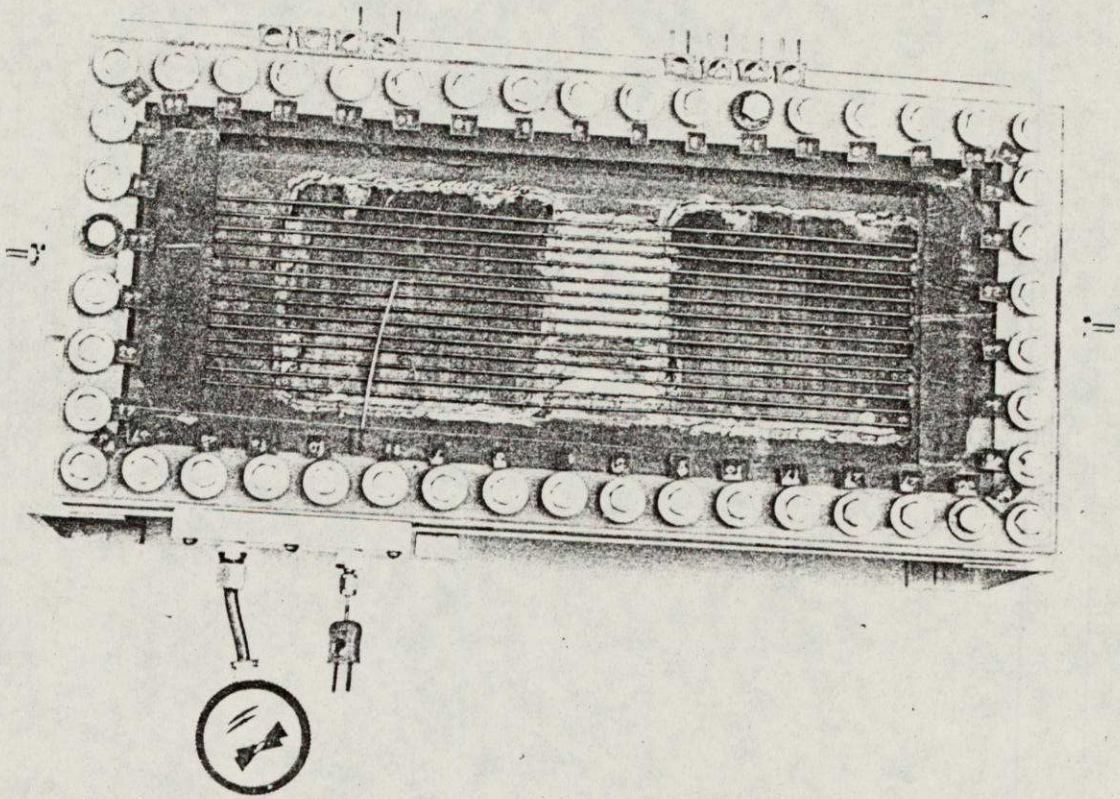

Figure 5. Top View of Assembled Heat Pipe.

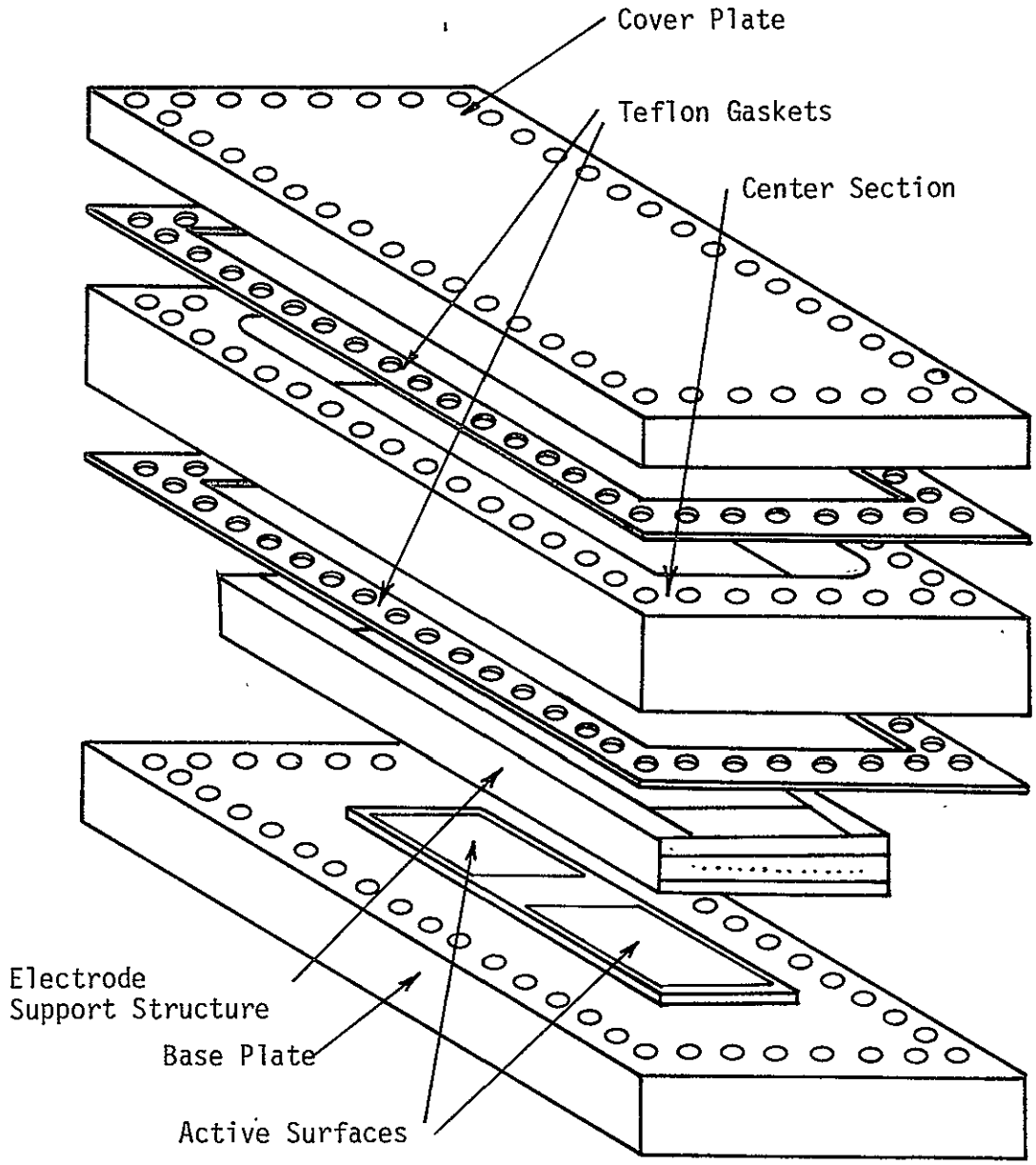

Figure 6. Heat Pipe Enclosure.

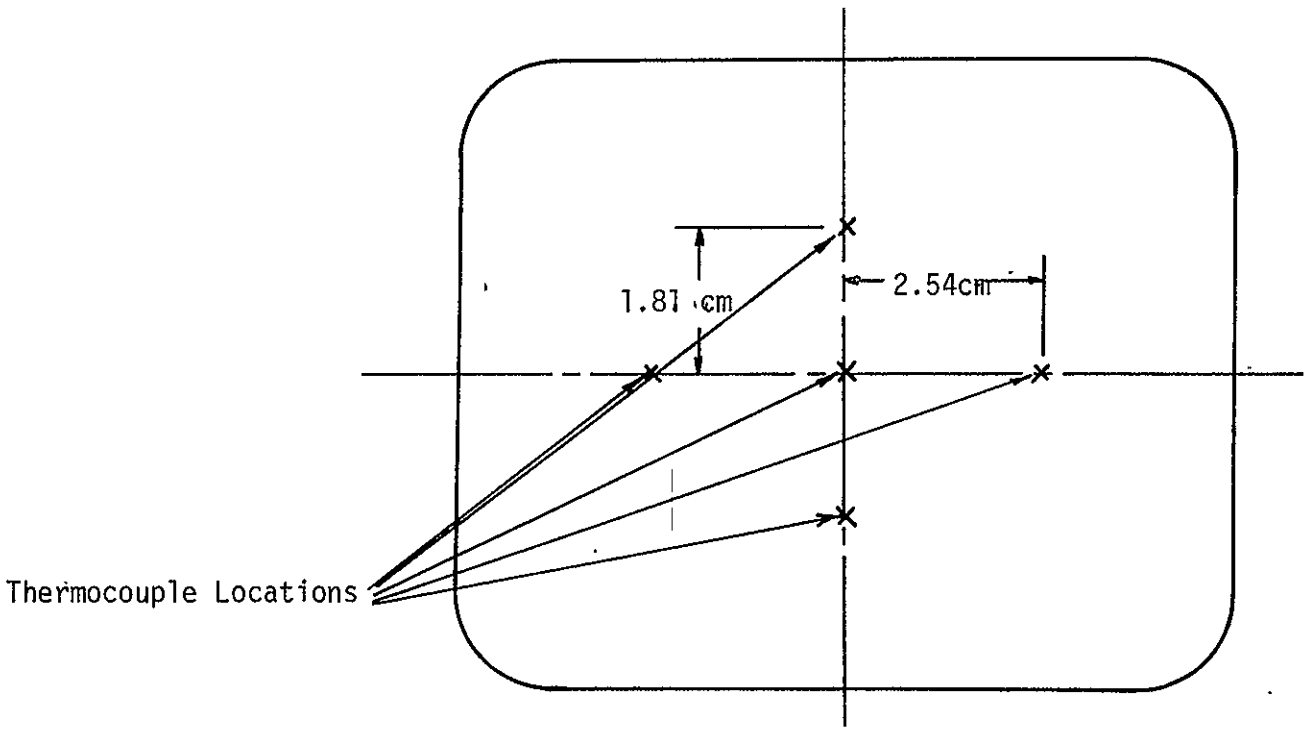

Figure 7. Locations of Thermocouples in Active Surfaces.

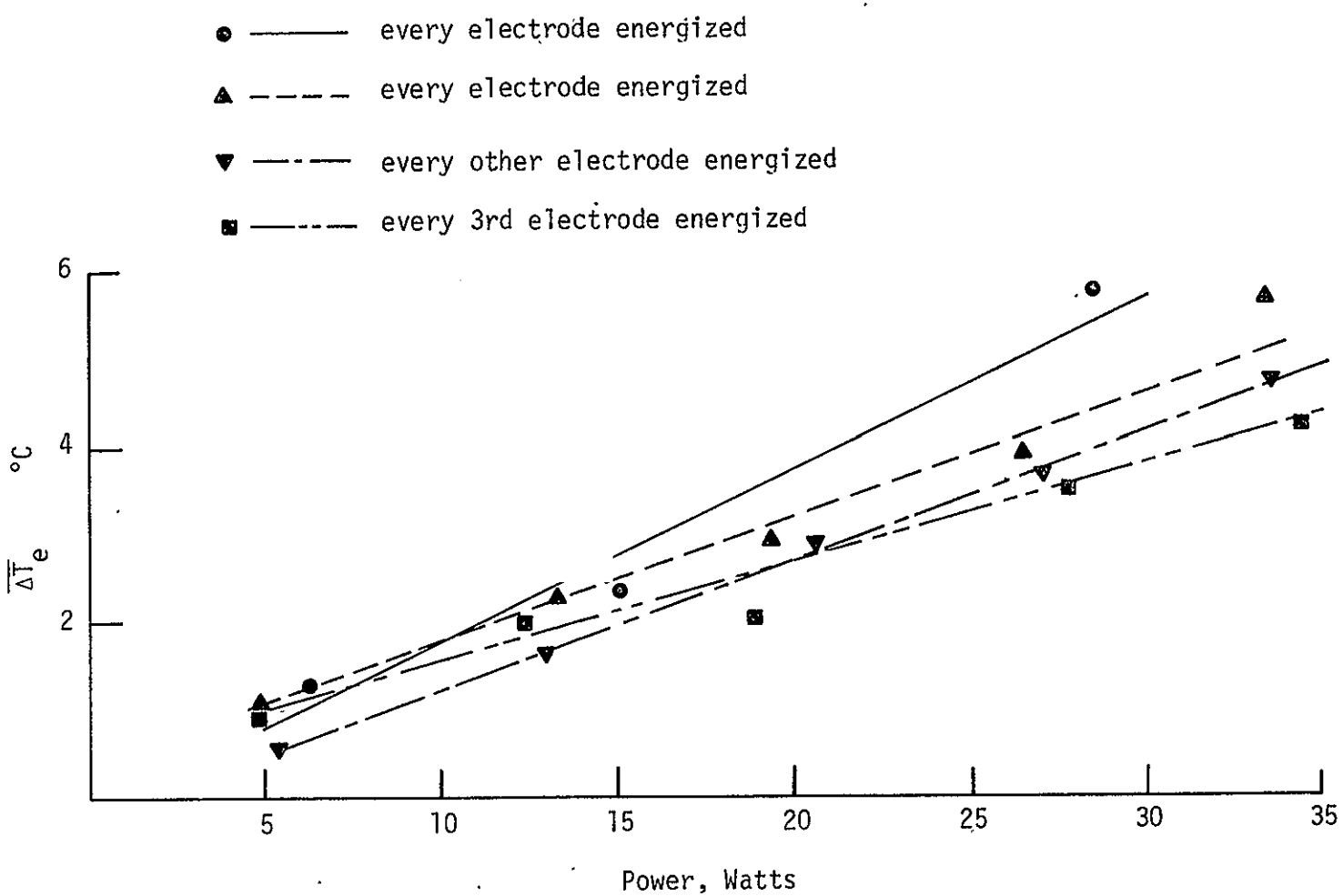

Figure 8. Evaporator Superheat vs. Power.

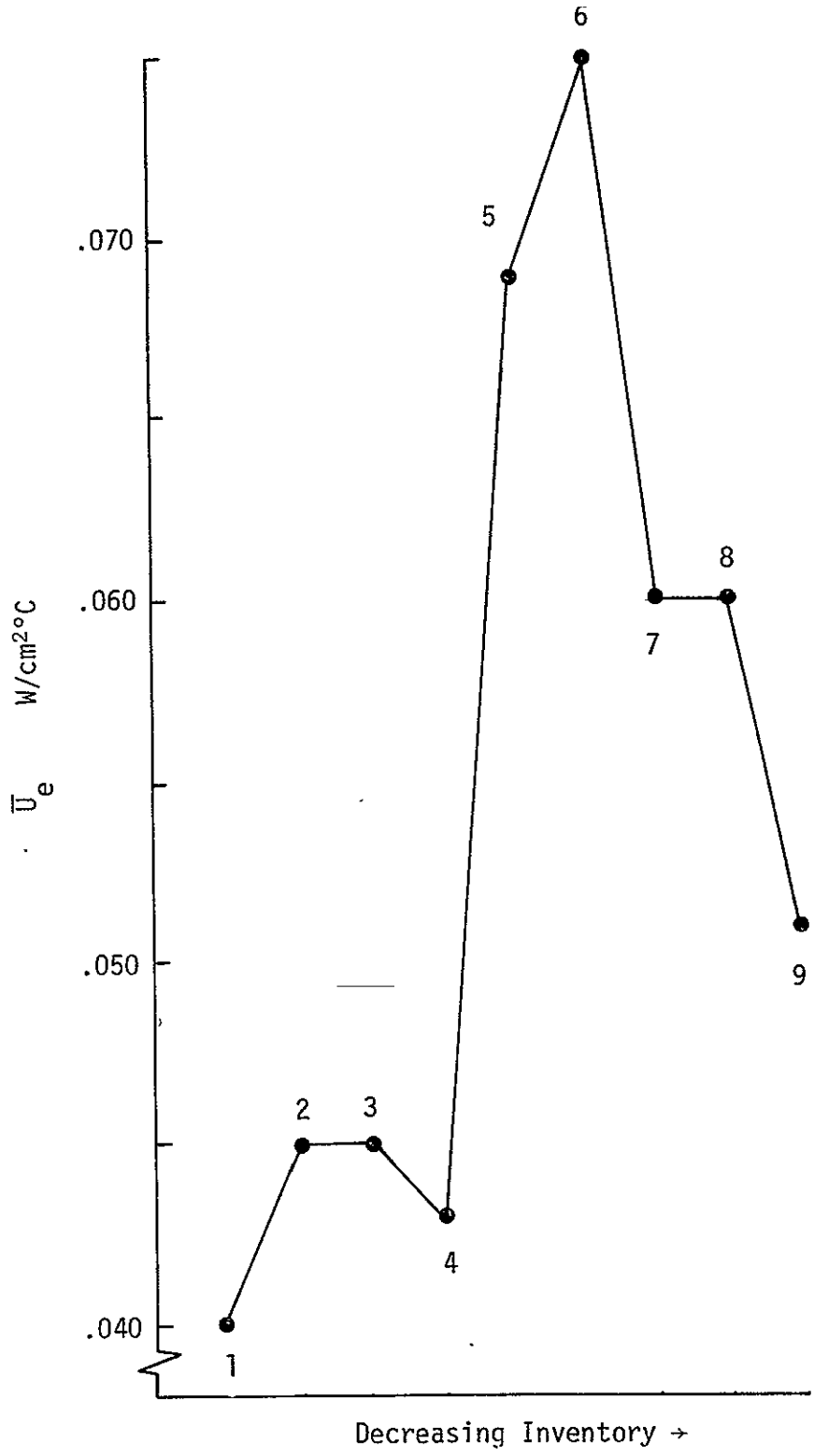

Figure 9. Qualitative Effect of Inventory on Evaporator Conductance.

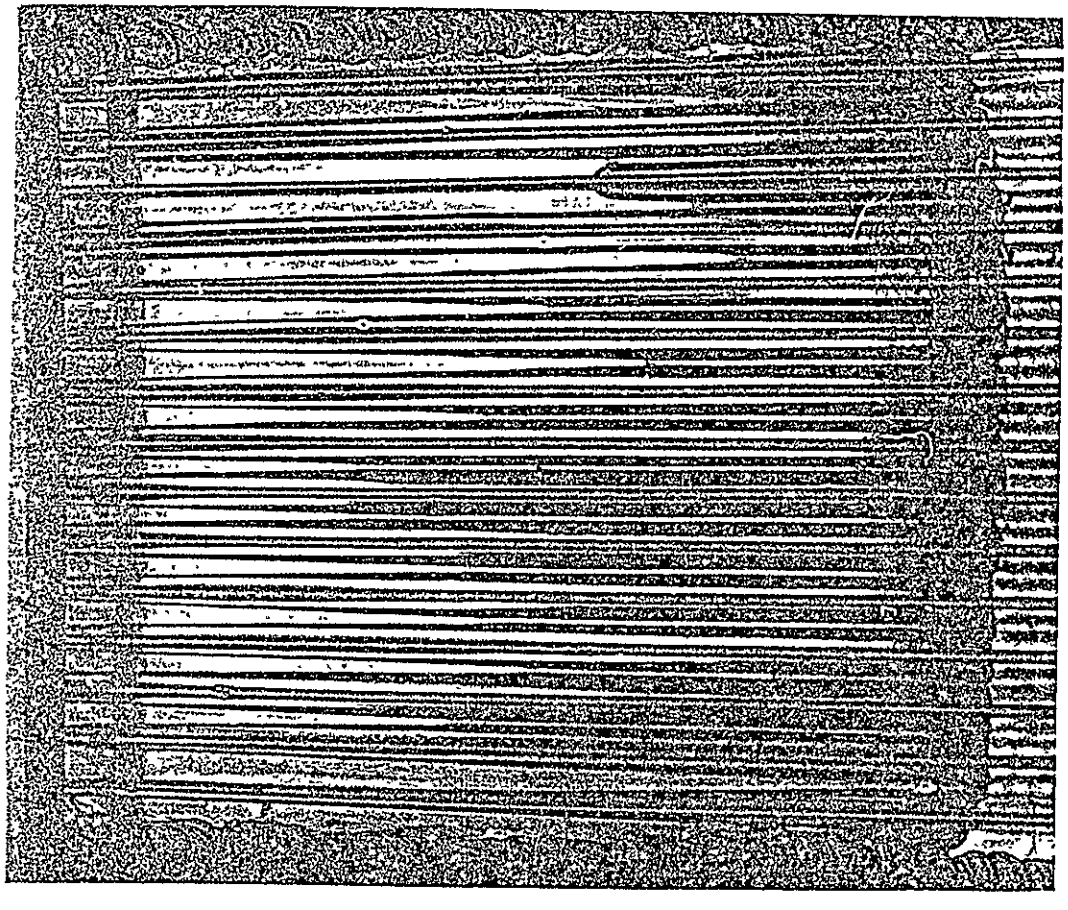

Figure 10. Smooth Evaporator Surface With Every Electrode Energized.

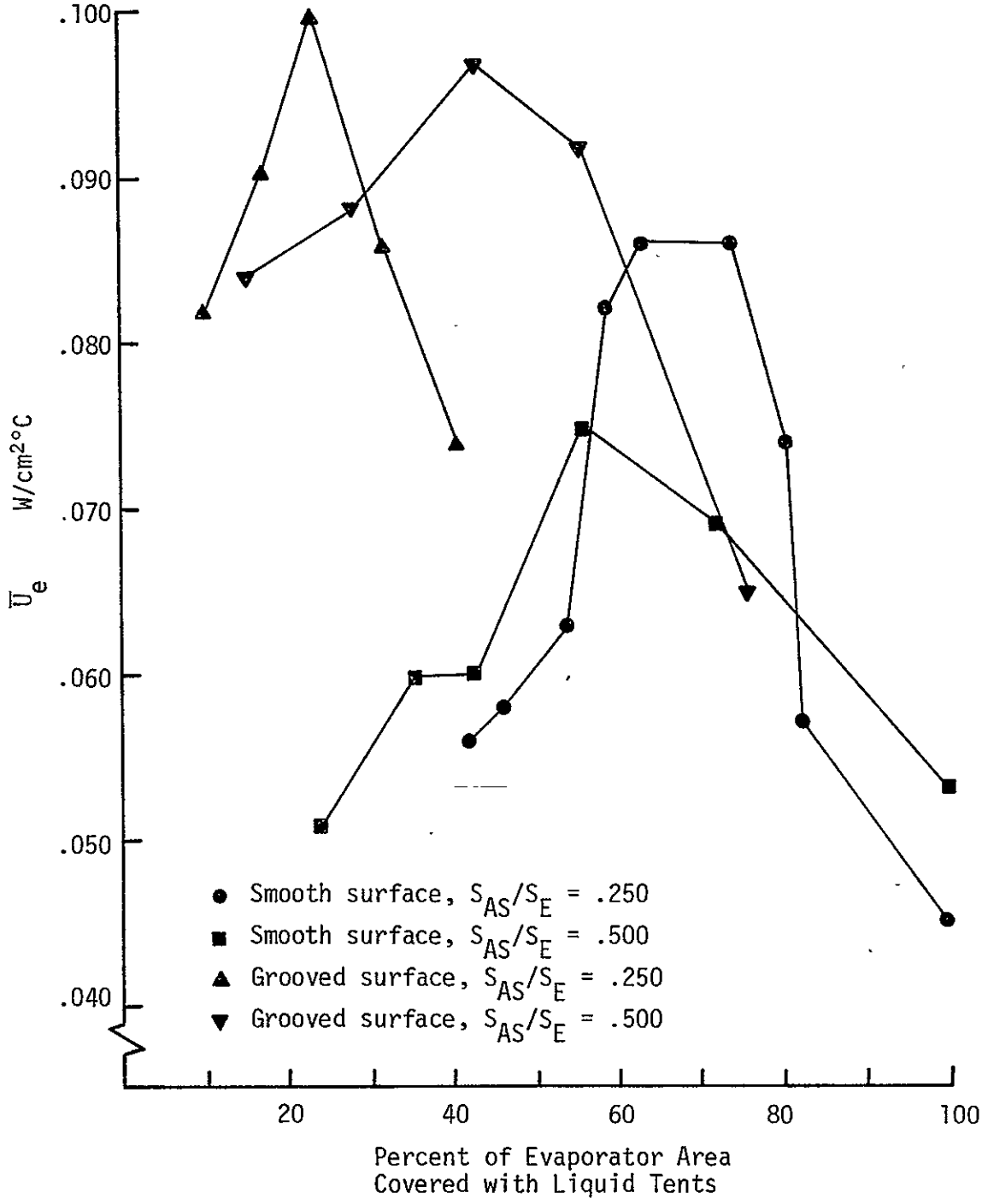

Figure 11 Quantitative Effect of Inventory on Evaporator Conductance.

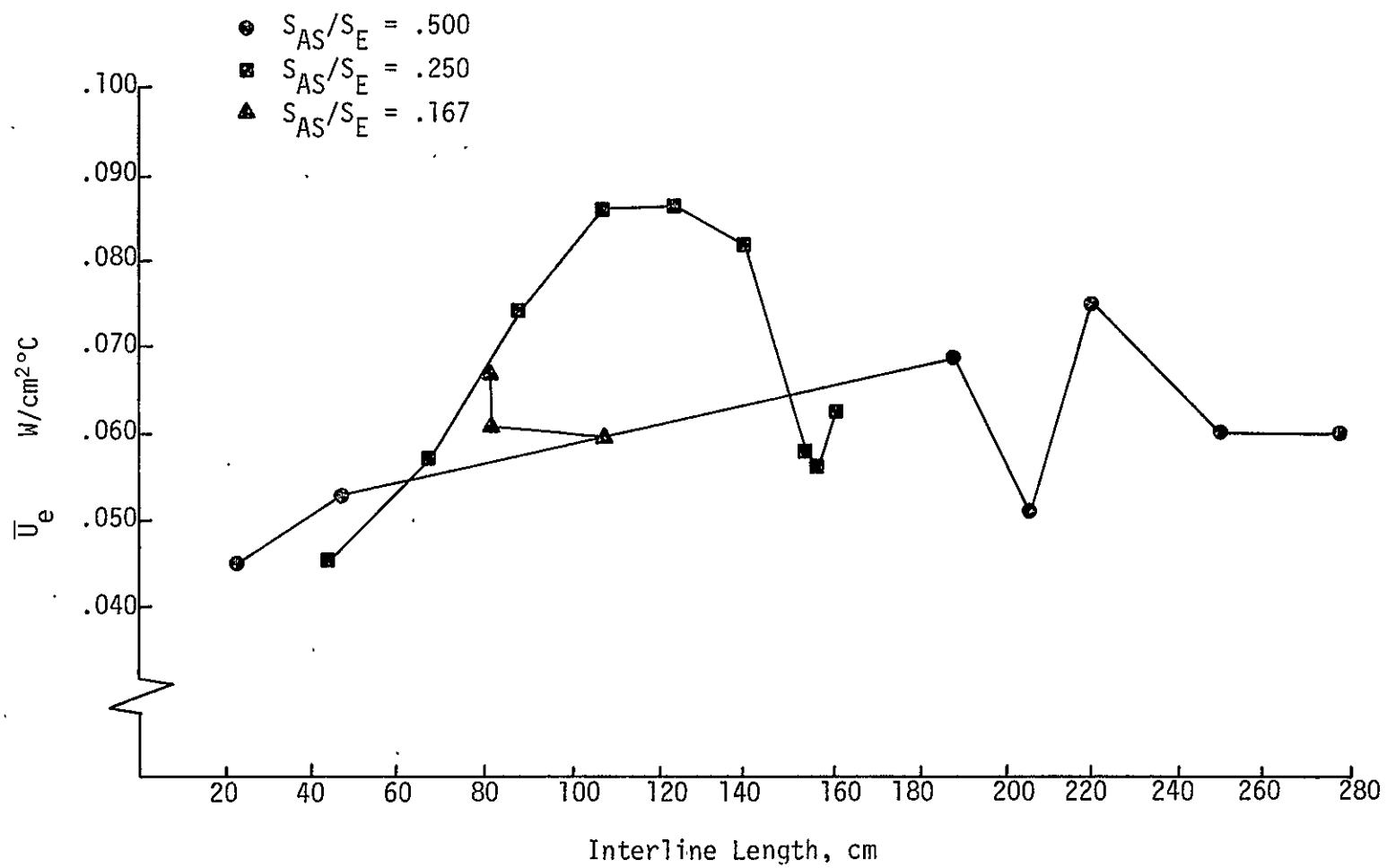

Figure 12. Effect of Interline Length on Evaporator Conductance.

LIST OF PUBLICATIONS
ISSUED DURING COURSE OF GRANT

1. Jones, T. B., "The Feasibility of Electrohydrodynamic Heat Pipes," Research Report #1, Electrical Engineering Dept., Colorado State University, NASA CR-114392, 1971.

2. Jones, T. B. and Perry, M. P., "Entrainment in Electrohydrodynamic Heat Pipes," Research Report #2, Electrical Engineering Dept., Colo. State University, NASA CR-114499, 1972.

3. Jones, T. B. and Perry, M. P., "Experiments with an Electrohydrodynamic Heat Pipe," Research Report #3, Electrical Engineering Dept., Colo. State University, NASA CR-114498, 1972.

4. Jones, T. B. and Perry, M. P., "Electrohydrodynamic Heat Pipe Research," Research Report #4, Electrical Engineering Dept., Colo. State University, NASA CR-114646, 1973.

5. Jones, T. B., "An Electrohydrodynamic Heat Pipe," ASME paper 72-WA/HT-35, 1972.

6. Jones, T. B., "Electrohydrodynamic Heat Pipes," Int. J. Heat Mass Transfer, Vol. 16, pp. 1045-1048, 1973.

7. Jones, T. B. and Perry, M. P., "Electrohydrodynamic Heat Pipe Experiments," J. Applied Physics, Vol. 45, pp. 2129-2132, 1974.

8. Jones, T. B., "An Electrohydrodynamic Heat Pipe," Mechanical Engineering, Vol. 96, pp. 27-32, 1974.

9. Jones, T. B., "Hydrostatics and Steady Dynamics of Spatially-Varying Electromechanical Flow Structures," J. Applied Physics, Vol. 45, pp. 1487-1491, 1974.

10. Loehrke, R. I. and Debs, R. J., "Measurements of the Performance of an Electrohydrodynamic Heat Pipe," AIAA paper 75-659, 1975.

11. Loehrke, R. I. and Sebits, D. R., "Flat Plate Electrohydrodynamic Heat Pipe Experiments," Mechanical Engineering Dept., Colo. State University, NASA CR-137707, 1975.

12. Loehrke, R. I. and Debs, R. J., "Measurements of the Performance of an Electrohydrodynamic Heat Pipe," Progress in Astronautics and Aeronautics, Vol. 49, pp. 503-513, 1976.

13. Loehrke, R. I. and Sebits, D. R., "Flat Plate Electrohydrodynamic Heat Pipe Experiments," Proc. 2nd. International Heat Pipe Confr., pp. 103-110, 1976.